Realizing field-dependent conduction in ZnO nanowires without annealing

Conor P. Burke-Govey, Uli Castanet, Harry Warring, A. Nau, Ben J. Ruck, Jérôme Majimel, Natalie O. V. Plank

Realizing field-dependent conduction in ZnO nanowires without annealing

C. P. Burke-Govey[1,2], U. Castanet[3], H. Warring[1,2], A. Nau[3], B. J. Ruck[1,2], J. Majimel[3] and N. O. V. Plank[1,2]

[1] *School of Chemical and Physical Sciences, Victoria University of Wellington, Wellington 6021, New Zealand*
[2] *The MacDiarmid Institute for Advanced Materials and Nanotechnology, New Zealand*
[3] *CNRS, Univ. Bordeaux, ICMCB, UPR 9048, 87 Avenue du Docteur Schweitzer, F-33600 Pessac, France*

Abstract

We report on the low-temperature fabrication of field-effect transistors by bridging pre-patterned electrodes using ZnO nanowires grown *in situ*, which operate without requiring post-growth processing or annealing. The devices show good performance using as-grown nanowires, with on–off ratios of 10^5 and threshold voltages of 2 V. Electron microscopy shows the field-dependent nanowires hierarchically nucleate from larger ZnO nanorods, and both are oriented along a common *c*-axis. A high nanowire surface-to-volume ratio allows depleting electron traps on the nanowire surface to compensate intrinsic electron donors present throughout the nanowire bulk. This eliminates the need to reduce the electron concentration through high-temperature annealing, making the nanowires naturally field-dependent in their as-grown state.

1. Introduction

ZnO nanowires are a promising material for optoelectronic device fabrication at the nanoscale [1, 2]. In addition to being pseudo-1D semiconductors, ZnO nanowires are transparent in the visible spectrum due to their wide band gap (3.37 eV), and are also strongly piezoelectric. They can be easily synthesized using low-temperature hydrothermal methods [3, 4], which is desirable for growing nanowires directly *in situ* on delicate substrates for device fabrication.

However, as-grown nanowires are intrinsically n-type due to native electron donors, and their high electron concentration makes them unsuitable for use as field-effect transistors (FETs). This can be addressed by annealing the nanowires at high temperatures (typically 400 °C and above) [5–9] at the expense of losing the advantage of low-temperature synthesis. With future electronics trending towards the use of delicate substrates [10], low-temperature processes will be necessary for fabricating devices at the wafer scale. Further development of ZnO nanowire FETs will therefore benefit from being able to synthesize field-dependent nanowires *in situ*, whilst also taking full advantage of low-temperature processing and device fabrication [6].

Here, we report the low-temperature growth of ZnO nanowires *in situ* for FET fabrication, which operate without requiring post-growth processing or annealing. FETs are fabricated by directly growing ZnO nanowires between pre-defined electrodes using a polymer-assisted hydrothermal growth technique. The FETs show good device performance despite using as-grown nanowires, with on-off ratios of 10^5 and threshold voltages of +2 V. Persistent ultra-violet (UV) photoconductivity measurements show that depleting electron traps on the nanowire surface, coupled with a high surface-to-volume ratio,

compensate native electron donors in the nanowire bulk. These depleting trap states sufficiently lower the electron concentration to allow field dependency and FET compatibility, making it unnecessary to expel electron donors using conventional high-temperature annealing.

2. Experimental details

2.1. Substrate preparation

Patterned seed layers of ZnO/Ti (100/60 nm) were defined and deposited on 1.2 cm × 1.2 cm SiO_2 (100 nm)/p^+-Si wafers (Silicon Quest International) using standard photolithography and lift-off processing. The ZnO/Ti layers were both deposited using an HHV RF Magnetron Sputter Coater with Ar processing gas at room temperature. The Ti capping layer prohibits vertical nanowire growth and provides an electrical contact for device measurements, while the ZnO layer acts as a seed for hydrothermal growth. The ZnO/Ti regions were deposited with inter-electrode spacing ranging from 10 μm up to 80 μm, in 10 μm increments.

2.2. Polymer assisted hydrothermal growth

We use a one-pot hydrothermal growth to synthesize hierarchical ZnO nanorods and nanowires from pre-patterned seed layers. Aqueous growth solutions were first prepared in borosilicate glass bottles by thoroughly mixing 25 mM of $Zn(NO_3)_2$ (Sigma Aldrich, 98% purity), 25 mM of hexamethylenetetramine (Sigma Aldrich, 99% purity), and a variable amount of polyethyleneimine (Sigma Aldridch) in 250 ml of de-ionized (DI) water (≥18.2 MΩ cm). We varied both the PEI concentration and molecular weight, using PEI with molecular weights of 800 (linear, branched), 1300 (linear), and 2000 (linear) g mol^{-1}.

After the precursors were thoroughly mixed, each growth solution was placed in a water bath and left to pre-heat for 1 h at a constant temperature of 95 °C. Once preheated, patterned seed layers were submerged in the growth solutions for 19 h at a constant 95 °C. Upon removal, the wafers were rinsed with DI water (≥18.2 MΩ cm) and then dried with nitrogen at room temperature. The hydrothermal growth solution is not refreshed or interfered with at any step during the growth process.

2.3. Electron microscopy

Scanning electron microscopy (SEM) images of ZnO nanowires and FETs were taken using a Jeol JSM 6500 F operating at 15 kV.

For transmission electron microscopy (TEM) measurements, ZnO nanowires and nanorods were collected from growth substrates by using a scalpel, and then suspended in alcohol by ultrasonication. Drops of the suspension were then deposited onto a copper grid covered with a carbon film. This grid was finally air-dried for 15 min. TEM and high-resolution TEM observations were performed using a JEOL 2200 FS equipped with a field emission gun, operating at 200 kV and with a point resolution of 0.23 nm. High-resolution transmission electron microscopy (HRTEM) micrographs were acquired with a Gatan Ultrascan CCD 2k–2k and digital diffractograms were calculated using the Gatan Digital Micrograph program. In order to be representative and statistically meaningful, many images from several regions of various samples were recorded, and the most characteristic results are presented here. Due to the thickness of the nanorods, high-resolution TEM observations were almost exclusively performed on the nanorod terminating ends. Only electron diffraction (ED) patterns have been recorded all along the nanorods.

2.4. Electrical characterization

Electrical measurements were performed using an Agilent 4156 C parameter analyzer with a Rucker and Kolls probe station. Transfer characteristics were acquired by sweeping the gate voltage from −10 V to 10 V, and then returning to −10 V. All transfer characteristics were acquired in ambient atmosphere at room temperature. Drain–source voltages were kept at 1 V for the transfer characteristics. Threshold voltages were determined by extrapolating from the linear portion of the transfer curve.

Photoconductivity measurements were performed using 395 nm UV LEDs as an ultraviolet light source at an intensity of 8.8 mW cm^{-2}. This intensity was measured before and after each exposure to ensure that there was no fluctuation in power over the course of UV exposure. Samples were mounted on printed circuit boards in an evacuated vacuum cryostat with a CaF_2 window to allow for sample illumination. The chamber pressure was measured during electrical measurements, and decreased from an initial pressure of 5.56×10^{-4} to 1.2×10^{-4} mbar over a 35 h period. All electrical and photoconductivity measurements were acquired using an Agilent 4156 C parameter analyzer, and individual pairs of electrodes were contacted using copper wire and silver paint. All measurements were performed at room temperature.

3. Results and discussion

After the hydrothermal growth process is complete, two distinct types of ZnO nanostructures grow hierarchically from the pre-patterned substrates, despite the one-pot growth process only involving a single step. Large horizontal nanorods grow directly outwards from the exposed sidewall of the deposited ZnO layers. The tips of these large nanorods terminate in very fine secondary nanowires that lie flush against the SiO_2 surface. As the gaps between pre-patterned electrodes range from 10 to 80 μm on a single chip, the shorter channels are bridged by large nanorods which meet in the middle of the channel gap, while the longer channels are bridged by the secondary nanowires growing hierarchically from the nanorods. Vertical nanowire growth from the ZnO layers is prohibited by the Ti capping layers, which are also used as source and drain electrodes to pass current through the bridging nanorods or nanowires. Each bridged channel can then be used as a back-gated FET by using the SiO_2/p^+-Si substrate as a dielectric and gate electrode.

Figure 1(a) shows a schematic of a nanowire FET after the one-pot hydrothermal growth process. The channel gap is bridged by a lateral array of high aspect-ratio nanowires that have grown horizontally along the substrate surface. These high aspect-ratio nanowires nucleate hierarchically from larger nanorods growing directly from the ZnO sidewall, as shown in figure 1(b). The high aspect-ratio nanowires meet in the middle of the channel, bridging the source and drain electrodes. Figures 1(c) and (d) show corresponding SEM images of an actual device. The larger nanorods are from 150 to 300 nm in diameter and 10–25 μm in length. They project radially in a three dimensional brush-like structure, anchored to the exposed ZnO sidewall. High aspect-ratio nanowires, with diameters from 10 to 50 nm and lengths of up to 10 μm, emerge from the tips of these larger nanorods, as shown in figure 1(d).

HRTEM measurements show that the nanorods and nanowires are monocrystalline and oriented along the [001] *c*-axis (see supplementary information figure S1, available online at stacks.iop.org/NANO/28/124003/mmedia) Images of the nanowire/nanorod interface suggest that the nanowires nucleate and grow epitaxially from the nanorods. Figure 2(a) shows a nanowire growing from the side face of a nanorod, with the interface between the two highlighted. Figure 2(b) shows an HRTEM image of the highlighted interface, displaying a common *c*-axis orientation between the nanowire and nanorod. This shared orientation minimizes misfits and favors epitaxial nanowire growth, although there are small areas where the crystal orientation slightly deviates from the common *c*-axis. Figure 2(c) highlights these deviations at the interface, which appear as contrast variations in the micrographs. ED

patterns of the nanowire and nanorod portions of the interface are available in the supplementary information (see figure S2.)

Given the fact that our hydrothermal growth process only involves a single growth step, it is surprising that we see two distinct nanostructures growing heirarchically from the seed layers. The nucleation of hierarchical nanowires from larger nanorods only occurs for polymer assisted hydrothermal growth, when PEI is included in growth solution. While PEI is often used mainly as an additive that enhances nanowire aspect ratios [4], it has a complex effect on the reactions that drive nanowire growth [11]. Hierarchical nanowires were successfully grown using PEI molecular weights of 800, 1300, and 2000 g mol^{-1} (abbreviated as PEI(800), PEI(1300), and PEI(2000) respectively), with the overall yield of high aspect-ratio nanowires decreasing with increasing molecular weight. Each variety of PEI was initially used at a concentration of 2 mM, and was incrementally increased in subsequent nanowire growths.

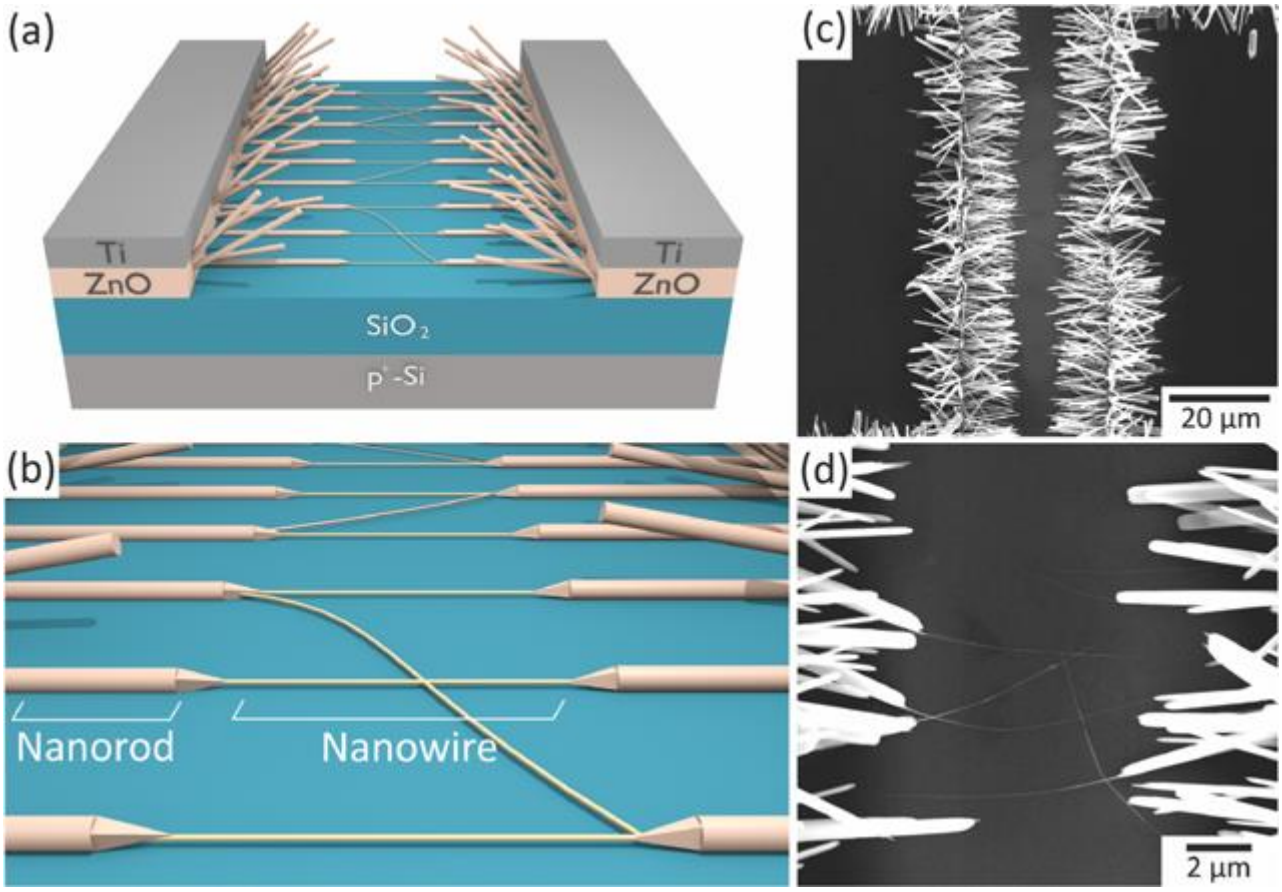

Figure 1. (a) A schematic of the patterned seed layers of ZnO/Ti deposited on the SiO_2/p^+-Si device substrate. ZnO nanorods project from the exposed ZnO sidewalls. (b) Smaller hierarchical ZnO nanowires nucleate from larger nanorods, bridging the ZnO/Ti seed layers. (c) A scanning electron microscope image of a device, with nanorods clearly visible. (d) A close-up of a bridged channel, with nanorods and nanowires clearly visible.

Eventually the excessive PEI concentration etched away the deposited ZnO layer, which has also been reported in the case of vertical nanowire growths [11]. This occurred at 5 mM for PEI(2000), 6 mM for PEI(1300), and 12 mM for PEI(800). Samples were imaged using SEM and analyzed using ImageJ to investigate the relationship between the number of secondary nanowires and the concentration of PEI. The concentrations corresponding to a maximum number of nanowires were found to be 3 mM, 4 mM, and 8 mM for PEI(2000), PEI(1300), and PEI(800), respectively. SEM images of nanorods and nanowires grown using different concentrations and molecular weights of PEI are shown in figure 3. FETs fabricated

with PEI(800) clearly show a higher density and number of secondary nanowires. Further details of these results are available in the online supplementary information.

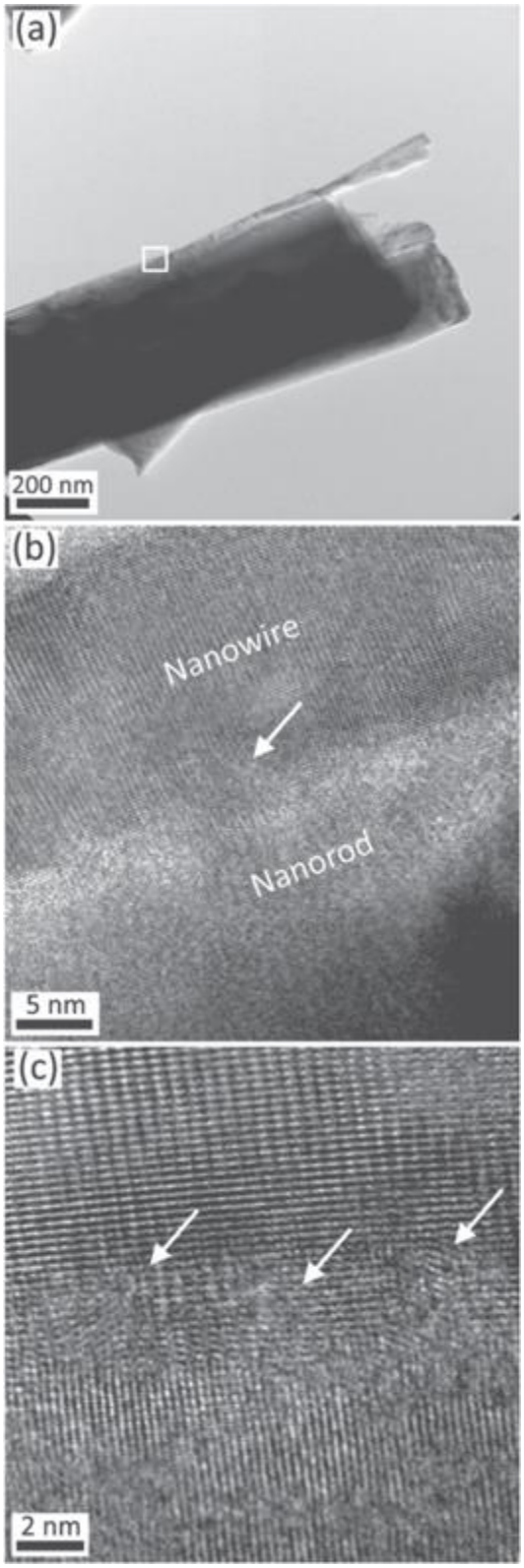

Figure 2. (a) Conventional bright field and (b), (c) HRTEM micrographs of a ZnO nanorod and nanowire interface. The interface strained regions are marked by arrows in (b) and (c).

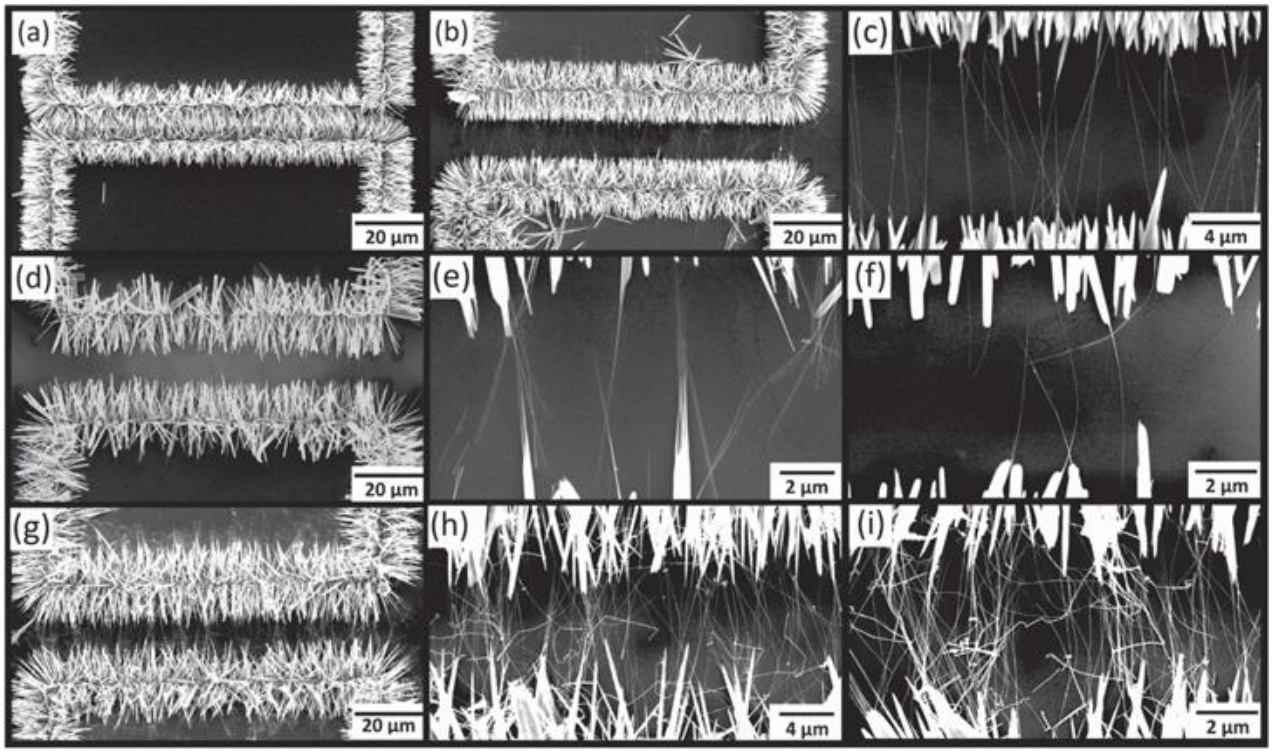

Figure 3. SEM images showing the morphology of synthesized ZnO NRs and NWs emerging from the edge of the ZnO/Ti dual seeds and electrodes. (a)–(c) Show the NRs and NWs grown with 3 mM of PEI (2000), (d)–(f) show the NRs and NWs grown with 4 mM of PEI (1300), and (g)–(i) show the NRs and NWs grown with 8 mM of PEI (800).

The field dependence of FETs bridged with high aspect-ratio nanowires was measured immediately after hydrothermal growth. The devices show a clear response to applied gate voltages, despite using unannealed as-grown nanowires. In contrast, FETs intentionally bridged with the larger nanorods do not respond to gate voltages, representative of the problem typically faced when using unannealed nanowires in FETs [5–9, 12]. Figure 4(a) shows I_{DS} versus V_G curves (transfer characteristics) for FETs bridged with high aspect-ratio nanowires and larger nanorods. The nanowire FET operates with a threshold voltage of 2 V, and an on–off current ratio of 10^5. Although the nanorods and nanowires have different volumes (which may affect their response to an applied gate voltage), the difficulty in gating the nanorod FETs is consistent with other examples of as-grown nanowires, even with diameters directly comparable to the nanowires here [5, 6].

All of the high aspect-ratio nanowires we measured show well-defined field dependence and FET compatibility, regardless of the molecular weight or concentration of PEI used in the nanowire growth (additional transfer characteristics for several FETs made using different concentrations and molecular weights of PEI can be found in the online supplementary information.) In the absence of any high-temperature annealing or processing, what causes the as-grown field dependence of the high aspect-ratio nanowires? Some of the FETs we have fabricated (such as FET 2 in figure S3 (b)) are depleted at zero gate voltage, despite the fact that unannealed as-grown nanowires are typically 'on' (highly conductive) at zero gate voltage and cannot be depleted even with strong negative gate biases. If the as-grown nanowires presented here have a lower electron concentration than usual, there must either be fewer intrinsic electron donors to begin with, or the intrinsic electron donors are compensated for by electron acceptors. As the nanowires have a high surface to volume ratio, it is possible to capture electrons from the bulk through surface traps. O− and OH− groups from the atmosphere preferentially adsorb on ZnO nanowire surfaces, depleting the nanowire by compensating intrinsic electron donors [13–16]. There is some

variation in the densities of the depleting surface states between nanowires, which can even occur between nanowires retrieved from the same growth batch [17]. This variation can affect the charge carrier density of the nanowires, which may be responsible for the variation of device characteristics between the nanowire FETs fabricated here. Surface states also strongly affect the hysteresis of nanowire FETs [18, 19], which may be responsible for the device hysteresis and variation thereof.

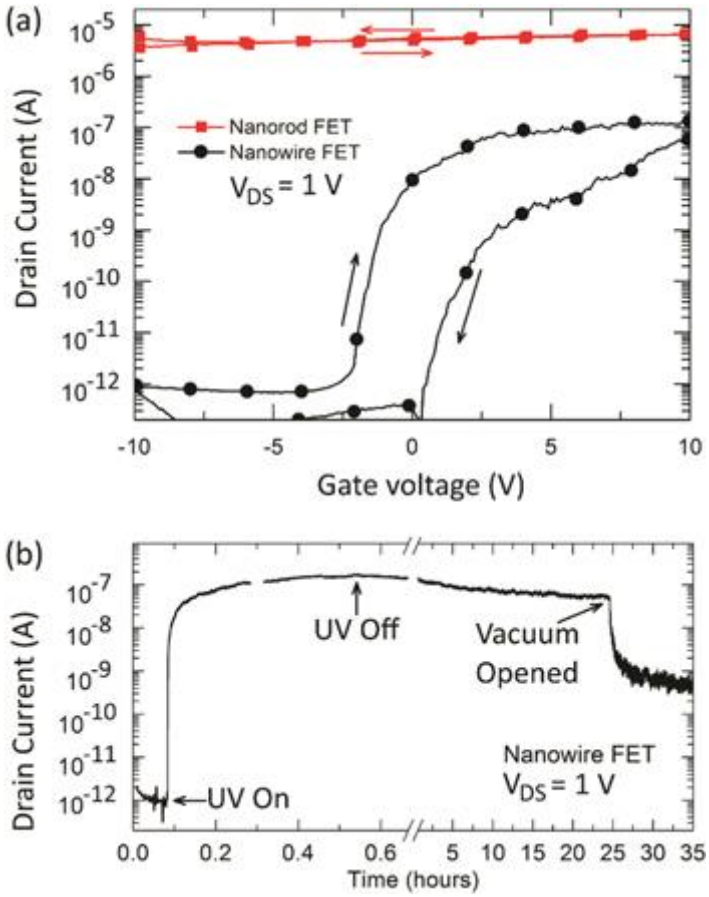

Figure 4. (a) Transfer characteristics of FETs bridged by nanowires (circles) and nanorods (squares). The nanowire FET shows strong field dependence, with a threshold voltage of 2 V and an on–off ratio of 10^5. In contrast, the nanorod FET does not display field dependence. (b) The UV response of a nanowire FET held at a constant V_{DS} of 1 V under vacuum. No gate voltage is applied for the photoconductivity measurement. The nanowire FET is fabricated using 3 mM of PEI(2000).

It has been well documented that the surface states which deplete ZnO nanowires can be desorbed using UV radiation, releasing trapped electrons back into the nanowire bulk [20–24]. Although there is still some contention over the exact mechanism [21], it is generally accepted that photogenerated holes from electron–hole pairs recombine with surface-trapped electrons, which then causes the surface species to desorb [15, 20, 24, 25]. Thus, if a nanowire is exposed to UV radiation while being kept under vacuum, desorbed surface species are pumped away before they can readsorb, giving rise to a persistent nanowire photoconductivity. The significance of the surface traps can then be determined by the magnitude of the persistent photoconductivity.

Figure 4(b) shows the persistent photoconductivity of a nanowire FET as it is exposed to UV radiation under vacuum. The FET is driven at a V_{DS} value of 1 V with no applied gate voltage, and shows an initial dark current of 10^{-12} A. After the UV source is switched on, the drain current rapidly increases by 5 orders of magnitude. Although the wavelength of UV used (395 nm) falls outside of the bandgap of bulk ZnO, we

clearly see a photoresponse corresponding to electron–hole pair production and surface species desorption, which agrees with other reports using similar wavelengths of light [26, 27]. The photoconductivity is very persistent while the vacuum is maintained, remaining stable 24 h after the UV source is switched off. Similar to other ZnO nanowire persistent photoconductivity experiments in vacuum [20], we do not see an immediate drop in the current after switching off the UV light, which suggests the photocarrier contribution to the photocurrent is minor. The indeterminate path length and width of our channel make analytical calculations impossible, but a similar order-of-magnitude calculation suggests that the photocarrier current may be as low as ~10^{-4} nA [20]. The lack of a sharp decrease in photoconductivity when turning off the UV illumination also corroborates with other persistent photoconductivity experiments in vacuum, even when using UV that falls within the bandgap of bulk ZnO [20, 28].

After venting to atmosphere, the drain current decreases by almost two orders of magnitude over 10 h. As oxygen initially re-adsorps on the NW surfaces, electrons are trapped and the surface is depleted. This bends the energy bands at the surface of the nanowire, which increases the surface potential barrier and reduces the rate of electron trapping/oxygen adsorption. The rate of oxygen reabsorption is therefore affected by the amount of oxygen already on the surface, which contributes to the shape of the decay curve seen after the vacuum is opened [22, 23, 29]. Although the FET does not return to its initial dark current over this timescale, other nanowires in vacuum have shown similarly long decay times previously [20, 28]. The final measured current is approximately 1% of the peak photocurrent; this small discrepancy could possibly be explained by environmental factors not directly linked to oxygen adsorption [23]. For example, very small differences in relative humidity can have large effects on the resistivity of ZnO nanowire networks [30], which could be present when venting from a vacuum to uncontrolled ambient atmosphere. We also see a slight increase in noise towards the end of the photoconductivity measurement, which is caused by a reduced sampling rate over a long timescale.

The persistent photoconductivity shows that the nanowire electron concentration rapidly increases by orders of magnitude as the depleting surface states are removed from the nanowire surface. The depleting surface states therefore act as a competing defect mechanism to the electron donors still present in the bulk of the nanowire, and play a critical role in the as-grown field dependency of the nanowires. Comparative photoconductivity measurements on nanorod FETs (found in online supplementary figure S6) show a significantly smaller photoresponse than the nanowires, which agrees with their lack of field dependence. Synthesizing field-dependent nanowires *in situ* without high-temperature annealing therefore relies on achieving a sufficiently high aspect-ratio to allow surface traps to compensate intrinsic electron donors.

4. Conclusion

In summary, we have used a polymer-assisted hydrothermal method to grow field-dependent ZnO nanowires *in situ* for FET fabrication, without requiring post-growth annealing. The high aspect-ratio nanowires have diameters from 10 to 50 nm and lengths of up to 10 μm, and hierarchically nucleate from larger ZnO nanorods. Both nanowires and nanorods are monocrystalline and share an epitaxial *c*-axis orientation at their interface. FETs using as-grown nanowires show clear switching behavior, with on–off ratios of 10^5 and a threshold voltage of 2 V. In contrast, FETs fabricated with larger nanorods are field independent due to excessive electron donors. Persistent photoconductivity measurements show that the nanowire field dependence is caused by their large surface-to-volume ratio and depleting electron traps on their surface. These surface states compensate intrinsic electron donors and reduce the electron concentration without high-temperature annealing, meaning the wires can be used as FETs in their as-

grown state. The low-temperature synthesis of intrinsically field dependent ZnO nanowires will allow for the fabrication of devices on delicate substrates, and other applications where low-temperature processing is required.

Acknowledgments

N. Plank acknowledges support from the Marsden fund, project number E1728. U Castanet and J Majimel thank the PLACAMAT platform for its electron microscopy facilities. The authors sincerely thank A Micolich (UNSW) for his useful discussions.

Reference

1. Wang Z L 2004 Zinc oxide nanostructures: growth, properties and applications J. Phys.: Condens. Matter **16** R829–58.
2. Yang P, Yan R and Fardy M 2010 Semiconductor nanowire: what's next? Nano Lett. **10** 1529–36
3. Vayssieres L 2003 Growth of arrayed nanorods and nanowires of ZnO from aqueous solutions Adv. Mater. **15** 464–6.
4. Xu S and Wang Z L 2011 One-dimensional ZnO nanostructures: solution growth and functional properties Nano Res. **4** 1013–98.
5. Kälblein D, Weitz R T, Böttcher H J, Ante F, Zschieschang U, Kern K and Klauk H 2011 Top-gate ZnO nanowire transistors and integrated circuits with ultrathin self-assembled monolayer gate dielectric Nano Lett. **11** 5309–15.
6. Kälblein D, Ryu H, Ante F, Fenk B, Hahn K, Kern K and Klauk H 2014 High-performance ZnO nanowire transistors with aluminum top-gate electrodes and naturally formed hybrid self-assembled monolayer/AlOx gate dielectric ACS Nano **8** 6840–8.
7. Opoku C, Dahiya A S, Oshman C, Daumont C, Cayrel F, Poulin-Vittrant G, Alquier D and Camara N 2015 Fabrication of high performance field-effect transistors and practical Schottky contacts using hydrothermal ZnO nanowires Nanotechnology **26** 355704.
8. Opoku C, Dahiya A S, Cayrel F, Poulin-Vittrant G, Alquier D and Camara N 2015 Fabrication of field-effect transistors and functional nanogenerators using hydrothermally grown ZnO nanowires RSC Adv. **5** 69925–31.
9. Park Y K, Choi H S, Kim J-H, Kim J-H and Hahn Y-B 2011 High performance field-effect transistors fabricated with laterally grown ZnO nanorods in solution Nanotechnology **22** 185310.
10. Nathan A et al 2012 Flexible electronics: the next ubiquitous platform Proc. IEEE **100** 1486–517.
11. Liu K, Wu W, Chen B, Chen X and Zhang N 2013 Continuous growth and improved PL property of ZnO nanoarrays with assistance of polyethylenimine Nanoscale **5** 5986.
12. Burke-Govey C P and Plank N O V 2013 Review of hydrothermal ZnO nanowires: toward FET applications J. Vac. Sci. Technol. B **31** 06F101.
13. Liao L, Lu H B, Li J C, He H, Wang D F, Fu D J, Liu C and Zhang W F 2007 Size dependence of gas sensitivity of ZnO nanorods J. Phys. Chem. C **111** 1900–3.
14. Ra H-W, Khan R, Kim J T, Kang B R, Bai K H and Im Y H 2009 Effects of surface modification of the individual ZnO nanowire with oxygen plasma treatment Mater. Lett. **63** 2516–9.
15. Li Q H, Liang Y X, Wan Q and Wang T H 2004 Oxygen sensing characteristics of individual ZnO nanowire transistors Appl. Phys. Lett. **85** 6389.
16. Fan Z, Wang D, Chang P-C, Tseng W-Y and Lu J G 2004 ZnO nanowire field-effect transistor and oxygen sensing property Appl. Phys. Lett. **85** 5923.
17. Lord A M, Maffeis T G, Walton A S, Kepaptsoglou D M, Ramasse Q M, Ward M B, Köble J and Wilks S P 2013 Factors that determine and limit the resistivity of high-quality individual ZnO nanowires Nanotechnology **24** 435706.
18. Goldberger J, Sirbuly D J, Law M and Yang P 2005 ZnO nanowire transistors J. Phys. Chem. B **109** 9–14.

19. Hong W-K, Jo G, Kwon S-S, Song S and Lee T 2008 Electrical properties of surface-tailored ZnO nanowire field-effect transistors IEEE Trans. Electron Devices **55** 3020–9.
20. Bao J, Shalish I, Su Z, Gurwitz R, Capasso F, Wang X and Ren Z 2011 Photoinduced oxygen release and persistent photoconductivity in ZnO nanowires Nanoscale Res. Lett. **6** 404.
21. Liao Z-M, Lu Y, Xu J, Zhang J-M and Yu D-P 2009 Temperature dependence of photoconductivity and persistent photoconductivity of single ZnO nanowires Appl. Phys. A **95** 363–6.
22. Li Q H, Gao T, Wang Y G and Wang T H 2005 Adsorption and desorption of oxygen probed from ZnO nanowire films by photocurrent measurements Appl. Phys. Lett. **86** 123117.
23. Li Y, Della Valle F, Simonnet M, Yamada I and Delaunay J-J 2009 Competitive .surface effects of oxygen and water on UV photoresponse of ZnO nanowires Appl. Phys. Lett. **94** 023110.
24. Soci C, Zhang A, Xiang B, Dayeh S A, Aplin D P R, Park J, Bao X Y, Lo Y H and Wang D 2007 ZnO nanowire UV photodetectors with high internal gain Nano Lett. **7** 1003–9.
25. Liu N, Fang G, Zeng W, Zhou H, Cheng F, Zheng Q, Yuan L, Zou X and Zhao X 2010 Direct growth of lateral ZnO Nanorod UV photodetectors with schottky contact by a single-step hydrothermal reaction ACS Appl. Mater. Interfaces **2** 1973–9.
26. Swanwick M E, Pfaendler S M-L, Akinwande A I and Flewitt A J 2012 Near-ultraviolet zinc oxide nanowire sensor using low temperature hydrothermal growth Nanotechnology **23** 344009.
27. Hullavarad S, Hullavarad N, Look D and Claflin B 2009 Persistent photoconductivity studies in nanostructured ZnO UV sensors Nanoscale Res. Lett. **4** 1421–7.
28. Cammi D and Ronning C 2014 Persistent photoconductivity in ZnO nanowires in different atmospheres Adv. Condens. Matter Phys. **2014** 2–7.
29. Sohn J I, Hong W-K, Lee M J, Lee T, Sirringhaus H, Kang D J and Welland M E 2009 The influence of surface chemical dynamics on electrical and optical properties of ZnO nanowire field effect transistors Nanotechnology **20** 505202.
30. Zhang Y, Yu K, Jiang D, Zhu Z, Geng H and Luo L 2005 Zinc oxide nanorod and nanowire for humidity sensor Appl. Surf. Sci. **242** 212–7.